Influence of shape and electric field on electron relaxation and coherent response in quantum-dot molecules

2007 J. Phys.: Condens. Matter 19 346216

(http://iopscience.iop.org/0953-8984/19/34/346216)

IOP PUBLISHING JOURNAL OF PHYSICS: CONDENSED MATTER

J. Phys.: Condens. Matter **19** (2007) 346216 (14pp) doi:10.1088/0953-8984/19/34/346216

Influence of shape and electric field on electron relaxation and coherent response in quantum-dot molecules

H Y Ramirez[1,3], A S Camacho[1] and L C Lew Yan Voon[2]

[1] Departamento de Física, Universidad de Los Andes, Carrera 1 No 18^a-10, Bogota, Colombia
[2] Wright State University, 3640 Colonel Glenn Highway, 45435 Dayton, OH, USA

E-mail: ha-ramir@uniandes.edu.co or hanzyrg@hotmail.com

Received 13 April 2007, in final form 20 June 2007
Published 24 July 2007
Online at stacks.iop.org/JPhysCM/19/346216

Abstract

We studied the effects of the confinement geometry and of external electric field on the electron dynamics of spherical and cylindrical double quantum dots. With an effective-mass approach, we found eigenenergies and envelope wave functions for finite confinement numerically. Using these energy states, we studied the response of the system to electric field pulses of different intensities, by calculating the density-matrix evolution in the high-delocalization regime, considering electron–electron and electron–acoustic phonon interactions, as a function of external DC electric field in the coupling direction. We obtained suitable conditions for coherent emission from cylindrically shaped dots, while in the case of spherically shaped dots, the scattering process is faster than the quantum beat oscillation.

(Some figures in this article are in colour only in the electronic version)

1. Introduction

Double-quantum-dot arrays are good candidates to be useful in the implementation of nanodevices both for optoelectronics and quantum computation [1, 2]. Tunability of eigenenergies and long lifetimes of coherent states are the main advantages of such systems [3, 4]. We explore the possibility of using double dots as emitters of coherent electromagnetic radiation, since the formation of molecular states in multi-dot systems by hybridization of individual-dot states gives rise to energy spectra with closely split levels where quantum-beat oscillations may be expected [5–8].

The main obstacles to obtaining coherent emission from quantum dots are the scattering by carrier–carrier and carrier–phonon interactions. Calculations and measurements of decoherence

[3] Author to whom any correspondence should be addressed.

Table 1. Material parameters [4, 32].

V (meV)	m^* matrix	m^* dot	D (meV)	c_s (nm ns^{-1})	K	ρ (g cm^{-3})	h_{14} (V nm^{-1})	ϵ
500	0.0962 m_e	0.063 m_e	8600	5040.4	0.58	4.696	1.38	12.9

times in single quantum dots by electron–phonon interactions suggest that the lifetime of coherent states in these systems would be long enough to exceed the period of beating for interferences between energetically close states [9–11]. Electron–electron interactions have much larger scattering rates than the electron–phonon interactions when the electrons involved in the interaction are confined on the same dot [12], but this obstacle can be removed by controlling the quantum-dot carrier population, taking advantage of the fact that today, it is actually possible to have one-electron dots [13, 14].

On the other hand, the tunability of states, a highly desirable feature for applications, has been reached in double quantum dots using electrical bias as the control parameter, with the prediction of anticrossing regions or a high delocalization regime (HDR) by reaching conditions when there exists a high interaction between individual-dot states [15, 16]. Such a coupling between dots is a direct consequence of electronic tunneling through the interfaces of the confined systems, which is due to the finiteness of the confinement potential. That is the reason why we are interested in studying finite confinements while the most of the works on coupled dots are made considering infinite confinement [17–20]. On the other hand, extensive studies on quantum-dot molecules have been done for entanglement and luminescence, involving interband or several-electron interactions [21–23], while there are many fewer studies on intraband phenomena despite the large applicability of such a physics for devices [24–26] in which the complication of the carrier–carrier interaction is removed.

Using a dynamical one-electron model for perturbative scattering coupling [27], we studied here the most symmetrical geometries, which are spheres and cylinders. The degeneracy of the single-dot states of the shapes considered implies the involvement of several excited levels. In this work we dealt with the first five confined energy levels of the whole double-dot system. Although cylindrical and spherical dots have been barely reported in the literature as an experimental achievement [28, 29], such geometries are very fundamental and important in order to understand theoretically the physics of confined systems [30, 31].

In the first section we present the eigenenergies and envelope wave functions of single and double dots in each of the geometries studied. After that, we calculate the decay rates by electron–electron and electron–phonon interaction at room temperature, in order to obtain the density matrix evolution of the system after the application of an external pulse and to evaluate the total dipole moment, looking for the viability of coherent emission from the double-dot systems.

To the best of our knowledge, this is the first dynamical approximation for double quantum dots with finite confinement comparing the shape effects and using computed decoherence times.

2. Energy states and coupling between dots

The systems we focus on are pairs of quantum dots of different size, close enough to be electronically coupled, which is equivalent to having their individual states hybridized. They are chosen as islands of GaAs embedded in an $Al_{0.4}Ga_{0.6}As$ matrix. Material parameters are as in table 1. The confinement potential is modeled as a finite potential step. We consider spherical and cylindrical geometries. The case with cylindrical shape has two options: stacked

or lateral coupling. These two configurations are expected to have different behavior since, in the latter one, the axial symmetry is broken.

We found the energy levels by solving numerically the BenDaniel-Duke equation

$$\left[\frac{-\hbar^2}{2}\nabla\cdot\left(\frac{1}{m^*(x,y,z)}\nabla\right)+V(x,y,z)\right]\Psi(x,y,z)=E\Psi(x,y,z), \qquad (1)$$

where m^* is the electron effective mass, V is the offset in the conduction band of the two materials, e is the elemental charge, Ψ is the one-electron envelope function and E is the eigenenergy. This model is valid for the conduction states of $Al_xGa_{1-x}As$ since the band mixing is small because of its wide band gap [33].

In this report, we work with the first two energy values of individual spherical dots and the first three of cylindrical dots. The individual spherical dots have a non-degenerate ground eigenenergy and a three-fold degenerate first excited eigenenergy. The individual cylindrical dots also have a non-degenerate ground level and first excited eigenenergy, but a two-fold degenerate second excited energy value close to the former one. So, in both cases, to work with coupled dots with these levels hybridized it is necessary to consider a five-level system: one associated with the smaller dot and four with the bigger one. Figures 1(a)–(e) show the density of probability of the studied levels of a single dot for both considered geometries. Figure 1(f) shows the change of the energy values with the change of the size of the dots. In this work, in order to maintain geometric proportion, we use a length twice the radius for cylindrical dots guaranteeing regular cylinders, far away from the disk or wire limits.

For double dots we solved equation (1) with the term eFx added to the Hamiltonian nonperturbatively, where F is the external bias field and x the coordinate in the direction of the coupling between dots [16]. We found the first five eigenenergies as a function of the electric field for a pair of dots where the size relation allows tuning the HDR with low fields, since the ground state of the smaller dot is close to resonance with the first excited states of the larger dot in spherical dots or with the first and second excited states of the larger dot in cylindrical dots. A volume ratio of ∼4.3 between the dots to reach the HDR when the smaller dots are around 300 nm^3 was determined, then we worked with dots of radius 4 nm and 6.5 nm respectively, both for spherical and cylindrical dots. We study three cases in this report: case 1: double spherical dots; case 2: laterally coupled double cylindrical dots; and case 3: vertically coupled double cylindrical dots. In all these three cases, the ground state of the double-dot system is basically the same as the ground state of the individual larger dots.

For case 1, the ground state of the smaller dot is hybridized with one of the three states of the larger dot whose energy value is the first excited state (which is three-fold degenerated),[4] while for cases 2 and 3, depending on the magnitude of the bias field, the ground state of the smaller dot is hybridized with the first excited state or with one of the two states of the larger dot whose energy value is the second excited state, which is two-fold degenerated.[5]

Figures 2(a)–(c) show the considered excited energy values of the double-dot systems as a function of the electrical bias for cases 1, 2 and 3, respectively. In these figures anticrossing regions are observed as evidences of the coupling between states. Such couplings clear the degeneration of the first excited level for spherical dots and of the second excited level for cylindrical dots. Figures 2(d)–(f) show the density of probability for cases 1, 2 and 3, respectively, in the HDR. It is clear that total delocalization of the electron along the two-dot system occurs [16, 27].

[4] For this first excited level there are three degenerated states, one along each axis. The state hybridized with the ground state of the smaller dot is the one whose symmetry axis is the same as the coupling direction.

[5] For this second excited level there are two degenerated states, one along each of two axes which are perpendicular to the cylinder axis. The state hybridized with the ground state of the smaller dot is the one whose symmetry axis is the same as the coupling direction for a laterally coupled dot.

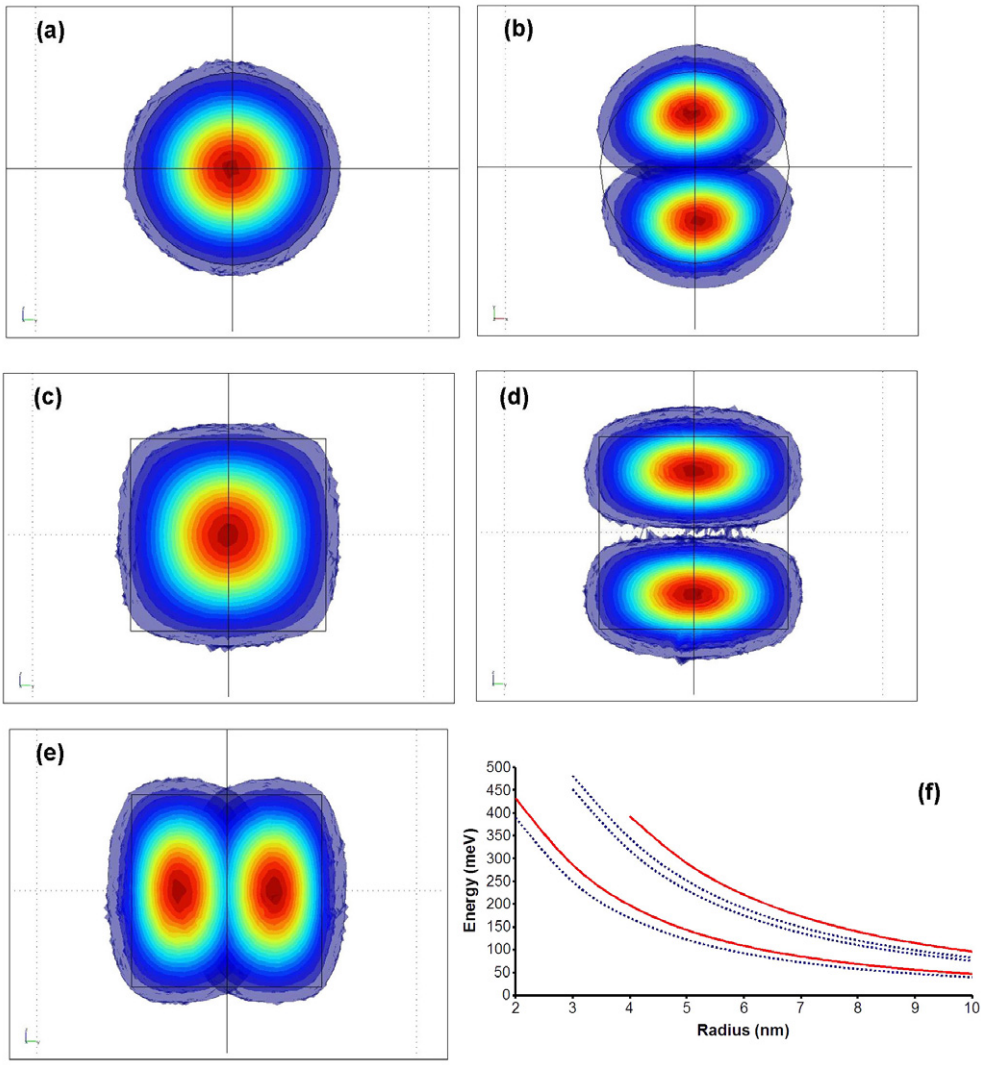

Figure 1. Electronic density of probability for spherical quantum dots: (a) ground state, (b) first excited state (three-fold degenerated); and cylindrical quantum dots: (c) ground state, (d) first excited state, (e) second excited state (two-fold degenerated). (f) Eigenenergies changing with the size of the dots (solid: spherical dots, dashed: cylindrical dots).

3. Electron–acoustic-phonon interaction

We calculated the decay rates for transitions induced by phonons of long wavelength. As shown in figures 2(a)–(c), the transition energies between excited levels do not include values close to the longitudinal optical phonon (∼36 meV) [4]. It has been discussed that the polar coupling in zero-dimensional (0D) structures is relevant [34, 35], but the experimental evidences show that the interaction between two states is appreciable only close to the crossing region between the lower state with the phonon and the upper one without the phonon [36, 37]. As a consequence, we considered only electron–acoustic-phonon interactions.

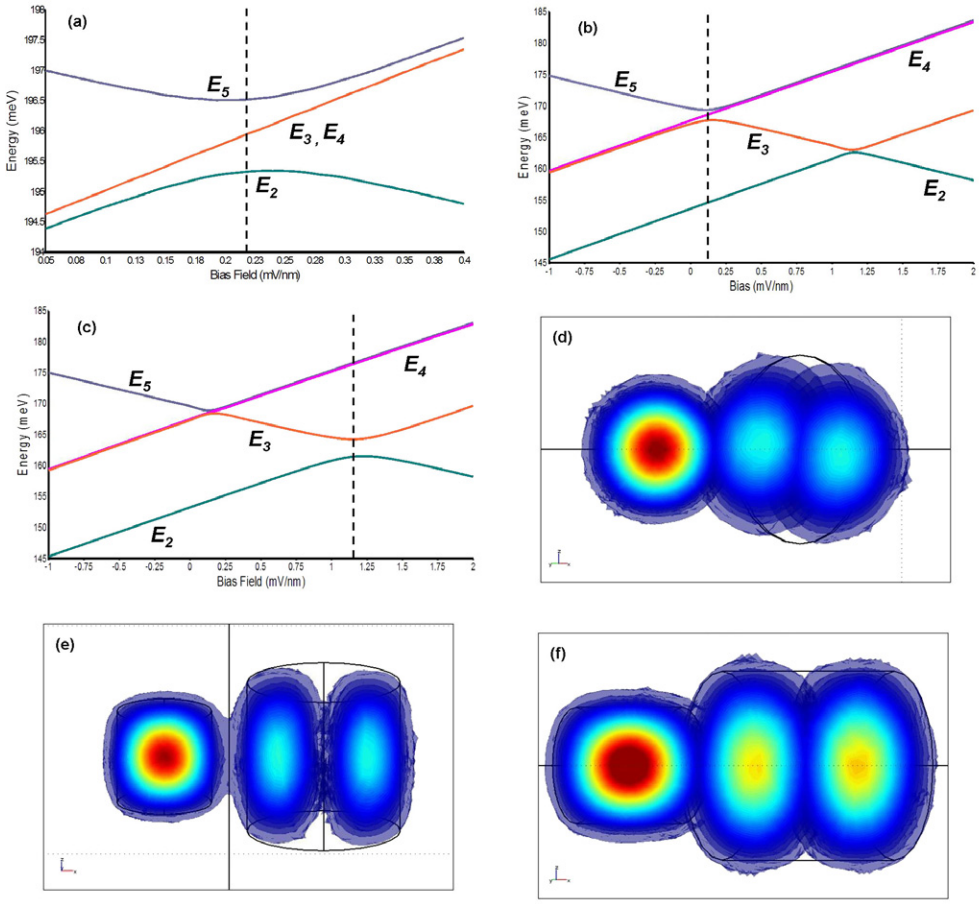

Figure 2. Considered excited energy values of double-dot systems as a function of the bias field for (the fixed distance between the centers of the dots is 13.5 nm): (a) case 1 (spherical double quantum dots), (b) case 2 (laterally coupled double cylindrical quantum dots) and (c) case 3 (vertically coupled double cylindrical quantum dots); the dashed vertical lines indicate the anticrossing considered in each case. Electronic density of probability of the first delocalized state for: (d) case 1 ($F = 0.22$ mV nm^{-1}), (e) case 2 ($F = 0.125$ mV nm^{-1}), and (f) case 3 ($F = 1.25$ mV nm^{-1}).

In this and in the next section, the decay rates between an initial state (i) and a final state (f) were calculated using the Fermi golden rule (FGR) approximation by solving numerically

$$\Gamma_{\mathrm{if}} = \frac{2\pi}{\hbar} |H_{\mathrm{if}}|^2 \, \delta(E), \tag{2}$$

where Γ_{if} is the scattering rate for transition between the states i and f, $\delta(E)$ imposes the energy conservation in the transition and $|H_{\mathrm{if}}|$ is the matrix element of the interaction electron–phonon by deformation potential (e–p-D), electron–phonon by piezoelectric potential (e–p-P) or electron–electron (e–e). The use of the FGR approximation has been questioned in the cases when the coupling is strong [38]; however, for the kind of system we are studying here, such an approximation is justified for times around picoseconds or longer [39, 40].

We calculated decay rates by deformation and piezoelectric potential interactions using a Fröhlich Hamiltonian

$$H^{\text{e-p-D}} = \sum_{\vec{q}} B_q^{\text{D}} \rho(\vec{q})(a_{\vec{q}} + a_{-\vec{q}}^{\dagger}),$$
$$H^{\text{e-p-P}} = \sum_{\vec{q}} B_q^{\text{P}} \rho(\vec{q})(a_{\vec{q}} + a_{-\vec{q}}^{\dagger}), \tag{3}$$

where the $a^{\dagger}(a)$ are the bosonic creation (annihilation) operators, $\vec{q}$ is the transferred momentum, $\rho(\vec{q})$ is the electronic density operator, and B_q^{D} (B_q^{P}) is the coefficient of the deformation (piezoelectric) interaction according to [41]:

$$B_q^{\text{D}} = D\left(\frac{\hbar}{2Mc_{\text{S}}|\vec{q}|}\right)^{\frac{1}{2}}|\vec{q}|\,, \qquad B_q^{\text{P}} = \frac{B_q^{\text{D}}}{D\,|\vec{q}|}(eh_{14})^2\left(\frac{12}{35}+\frac{16}{35\kappa}\right), \tag{4}$$

where D is the deformation potential, M is the mass of the whole sample, c_{S} is the longitudinal speed of sound in the material, h_{14} is the only non-vanishing piezoelectric constant, κ is the ratio between the transverse and longitudinal sound velocity, B_q^{D} is the deformation potential interaction coefficient, and B_q^{P} is the piezoelectric potential interaction coefficient after considering the average longitudinal and transverse contributions.

Introducing equations (4) in (3) we obtain the following final expressions for the deformation and piezoelectric potentials, respectively:

$$\Gamma_{\text{if}}^{\text{e-pD}} = \frac{T_{if,q_0} D^2 q_0^3 (n_{T,q_0}+1)}{2\hbar c_{\text{S}}^2 \rho (2\pi)^2}, \tag{5a}$$

$$\Gamma_{\text{if}}^{\text{e-pP}} = \frac{T_{if,q_0} q_0 (n_{T,q_0}+1) e^2 (h_{14})^2}{2\hbar c_{\text{S}}^2 \rho (2\pi)^2}\left(\frac{12}{35}+\frac{16}{35\kappa}\right), \tag{5b}$$

$$T_{\text{if},q_0} = \int_0^{2\pi}\int_0^{\pi} (I_{\text{if},\vec{q}_0})^2 \sin(\theta)\,\mathrm{d}\theta\,\mathrm{d}\varphi,$$

$$I_{\text{if},\vec{q}_0} = \int_{\text{All Space}} \mathrm{e}^{\mathrm{i}\vec{q}_0\cdot\vec{r}}\Psi *_{\text{f}} (\vec{r})\Psi_{\text{i}}(\vec{r})\,\mathrm{d}\vec{r},$$

with transferred momentum $q_0 = (E_{\text{i}} - E_{\text{f}})/\hbar c_{\text{S}}$; ρ is the material density, and n_{T,q_0} is the phonon occupation number depending on the temperature and the transferred momentum. Since thermal excitations do play the most important role in the decoherence process, we work at room temperature (300 K) in order to check the real possibility of finding long coherent times in a normal phonon environment [27]. The total volume of the samples is around 4×10^5 nm^3.

Figures 3(a)–(c) show the relaxation times from equation (5*a*), and figures 4(a)–(c) the times from equation (5*b*) as a function of the bias field. These figures allow us to compare the orders of magnitude of the deformation and piezoelectric potential interactions. It is clear that the times associated with the piezoelectric potential are at least one order of magnitude larger that the times related to deformation potential. This is in agreement with those reported in [4, 42]. However, there is a discrepancy with those reported in [43], where the calculations were done basically in the small coupling regime. However, according to that result, when the coupling increases, the piezoelectric interaction decreases more quickly than the deformation one, and then our results could be expected in the high-coupling regime.

The curves are quite complicated, but some characteristics are clear. Around the points where there is maximum delocalization ($\sim$0.22 mV nm^{-1} for spherical dots, 0.125 and 1.25 mV nm^{-1} for lateral and vertical cylindrical dots respectively—see figure 2), the graphics present their main features. Most of the crossings between decay times happen at those points, because of the interchange of the symmetries of the wavefunctions just at these values. The strongest oscillations are found also at those points where the double-dot character influences

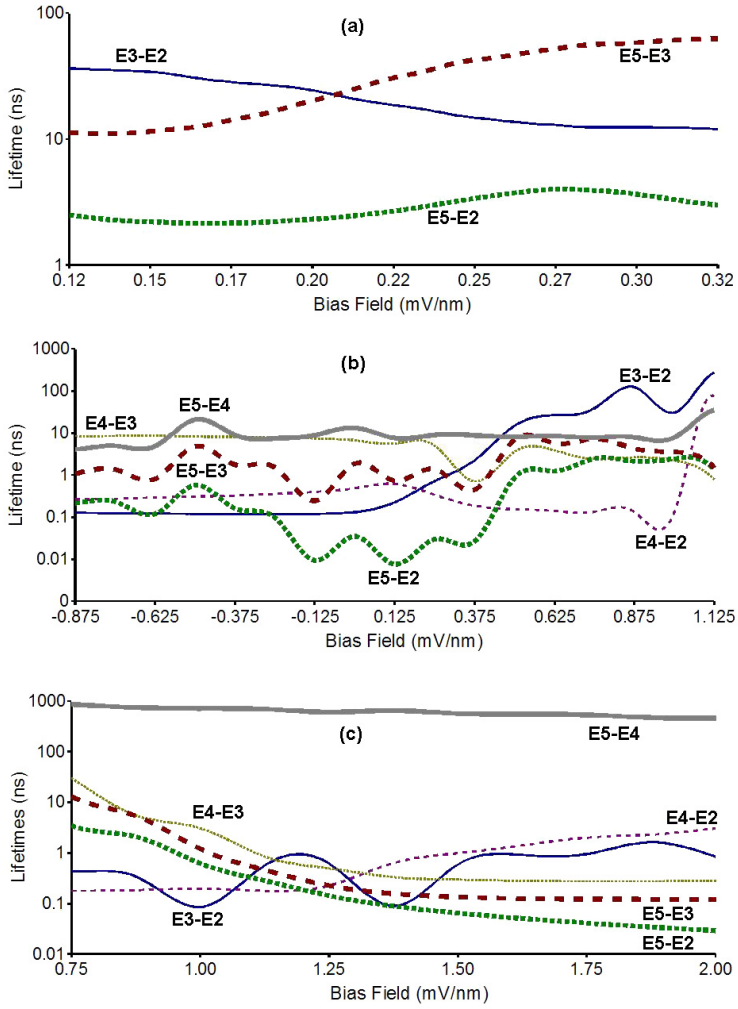

Figure 3. Electron–phonon decay times as a function of the bias field by deformation potential for transitions between excited levels: $E2$, $E3$, $E4$ and $E5$ (the transition corresponding to each line is indicated in the plots). (a) Case 1 (spherical double quantum dots), (b) case 2 (laterally coupled double cylindrical quantum dots), and (c) case 3 (vertically coupled double cylindrical quantum dots).

the interaction. Oscillatory behavior has also been predicted for multiple-dot systems with infinite confinement in [6, 44].

In general, for most of the transitions the shortest decay times are obtained for laterally coupled cylindrical dots, followed by stacked coupled cylindrical dots, and finally the longest times are found for spherical dots. Then this suggests a relationship between the symmetry of the system and the magnitude of the coupling. The more symmetrical the system, the smaller is the electron–acoustic-phonon interaction. Similar behavior has been reported for elliptical dots compared with spherical ones in single dots [45]. In these calculations, case 1 is the most symmetric and case 2 the least. Case 3 is an intermediate level because it maintains the axial symmetry. Compared with the reported values for bigger single dots of the same material, the lifetimes found are between 2–3 orders of magnitude longer [46].

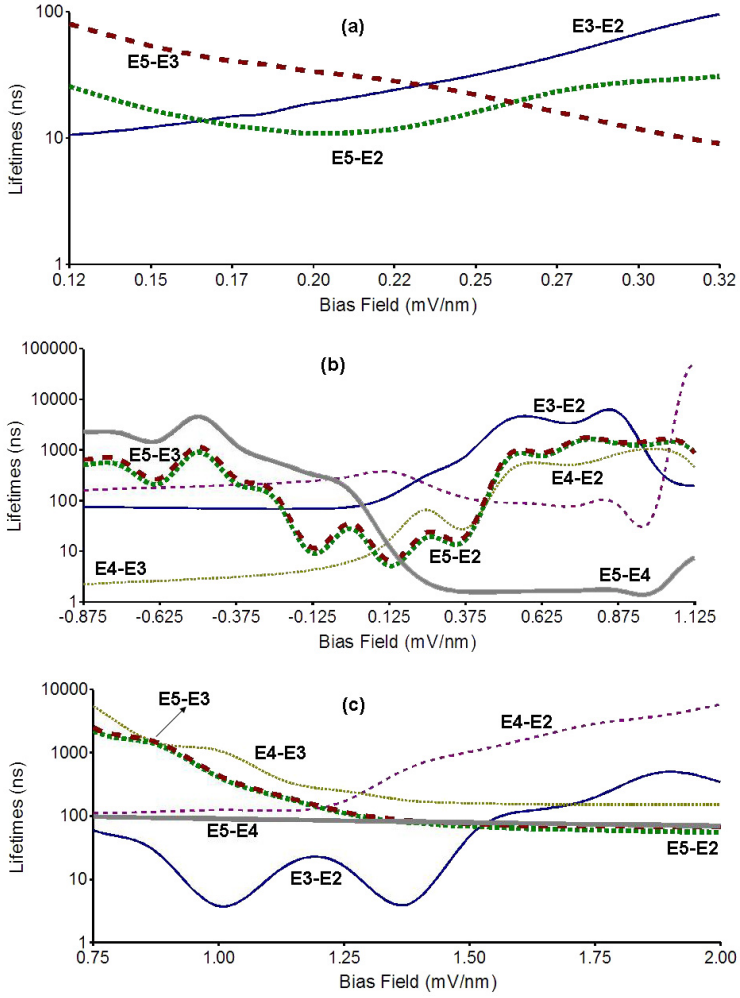

Figure 4. Electron–phonon decay times as a function of the bias field by piezoelectric potential for transitions between excited levels: $E2$, $E3$, $E4$ and $E5$ (the transition corresponding to each line is indicated in the plots). (a) Case 1 (spherical double quantum dots), (b) case 2 (laterally coupled double cylindrical quantum dots), and (c) case 3 (vertically coupled double cylindrical quantum dots).

4. Electron–electron interaction

A confined electron may interact with conduction electrons in the matrix material, and with other confined electrons. The scattering rates between confined electrons are expected to be higher than those between confined and 'free' electrons, because the spatial confinement makes the average separation shorter in the former case, as has been calculated for single quantum dots in [12]. In our case we assume just one confined electron, so only interaction with surrounding electrons is considered.

Again we use equation (2) to calculate the decay rates for this carrier–carrier interaction with the Hamiltonian

$$
\begin{aligned}
H^{\mathrm{e-e}} &= \sum_{\vec{q}} \frac{V_{\vec{q}}}{2\Omega} \sum_{klmn} C^{\dagger}{}_k C_l C_m^{\dagger} C_n I_{klmn}^{\vec{q}}, \\
V_q &= \frac{4\pi e^2}{q^2 \varepsilon}, \\
I_{klmn}^{\vec{q}} &= \int_{\text{All Space}} \Psi_k(\vec{r}_1) \Psi *_l (\vec{r}_1) \Psi *_m (\vec{r}_2) \Psi_n(\vec{r}_2) \mathrm{e}^{\mathrm{i}\vec{q}\cdot(\vec{r}_1 - \vec{r}_2)} \, \mathrm{d}\vec{r}_1 \, \mathrm{d}\vec{r}_2
\end{aligned}
\tag{6}
$$

where ε is the dielectric constant associated to the screening within the material, Ω is the total volume of the sample, C_{S}^{+} (C_{S}) is the fermionic creation (annihilation) operator in the state S, and $\Psi_{\mathrm{S}}(\vec{r}_n)$ is the wavefunction of the nth electron in the state S.

Inserting (6) in (2) and taking the average over all the directions, the final expression we used to calculate the decay rate for the transition of the confined electron between the state a (with energy Ea) and the state b (with energy Eb) by 'free'-electron–confined-electron interaction is

$$
\begin{aligned}
\Gamma_{ab}^{\mathrm{e-e}} &= \frac{e^4 G_{T,Ea,Eb}}{2L^2 \hbar \pi^3 (\Delta ab)^2 \varepsilon^2}, \\
G_{T,Ea,Eb} &= \int_{V_0}^{\infty} n f_{T,Ed} \tilde{I}_{a,b,c,d} \, \mathrm{d}E_d, \\
\tilde{I}_{a,b,c,d} &= \int_{\text{All Space}} \int_{\text{All Space}} C_1 C_2 \Psi_a(\vec{r}_1) \Psi_b^{\dagger}(\vec{r}_1) \mathrm{e}^{\mathrm{i}(\sqrt{2m*(\Delta ab + Ed)}/\hbar)\cdot\vec{r}_2} \mathrm{e}^{\mathrm{i}(\sqrt{2m*\Delta ab}/\hbar)\cdot\vec{r}_2} \, \mathrm{d}\vec{r}_1 \, \mathrm{d}\vec{r}_2
\end{aligned}
\tag{7}
$$

where V_0 is the confinement potential, $nf_{T,Ed}$ is the Fermi factor depending on the temperature and the variable energy of integration, Δab is the energy difference between the states a and b, C_1 and C_2 are constants of normalization of the wavefunctions of the 'free' electrons, and L is the average length of the sample. As with the electron–phonon interaction, we calculate the lifetimes at room temperature and use a free-carrier concentration of 10^{-18} nm^{-3}, typical of intrinsic $\mathrm{Al}_x\mathrm{Ga}_{1-x}\mathrm{As}$. Figures 5(a)–(c) show the decay times from equation (7) as a function of the bias field for the three cases considered.

From figure 5 it can be observed that this electron–electron interaction qualitatively, and for the most of the transitions, has an inverse behavior compared with the electron–phonon one. Whereas for electron–phonon interactions case 1 shows the longest times and case 2 the shortest ones, for electron–electron interactions case 1 has the shortest times and case 2 the longest ones. As in section 3, this could be related with the symmetry of the systems, although it is hard to conclude without more reference geometries. Again, besides the complexity of the shapes, especially in the cylindrical cases, the crossings of the curves in the high delocalization regions ($F = 0.22$ mV nm^{-1}, $F = 0.125$ mV nm^{-1} and $F = 1.25$ for cases 1, 2 and 3 respectively) are remarkable. To the best of our knowledge, no calculations for this kind of electron–electron interaction in double spherical or cylindrical quantum dots have yet been reported. According to our calculations, the sensitivity of the relaxation times to the shape of the dots is such that in spherical double dots the scattering by electron–electron interaction dominates over the electron–phonon one, contrary to what is usually believed about electron–phonon interaction being the main decoherence channel in quantum dots at finite temperature. The orders of magnitude and the trend of shorter times for more symmetric geometries agree with those reported by Nielsen for InGaAs quantum dots, where lens-shaped and cylindrical dots can be compared [47].

5. Dynamic response

The occupation probability of energy levels and the coherence between states for the reduced five-level system after the application of an ultra-fast electric field pulse can be obtained from

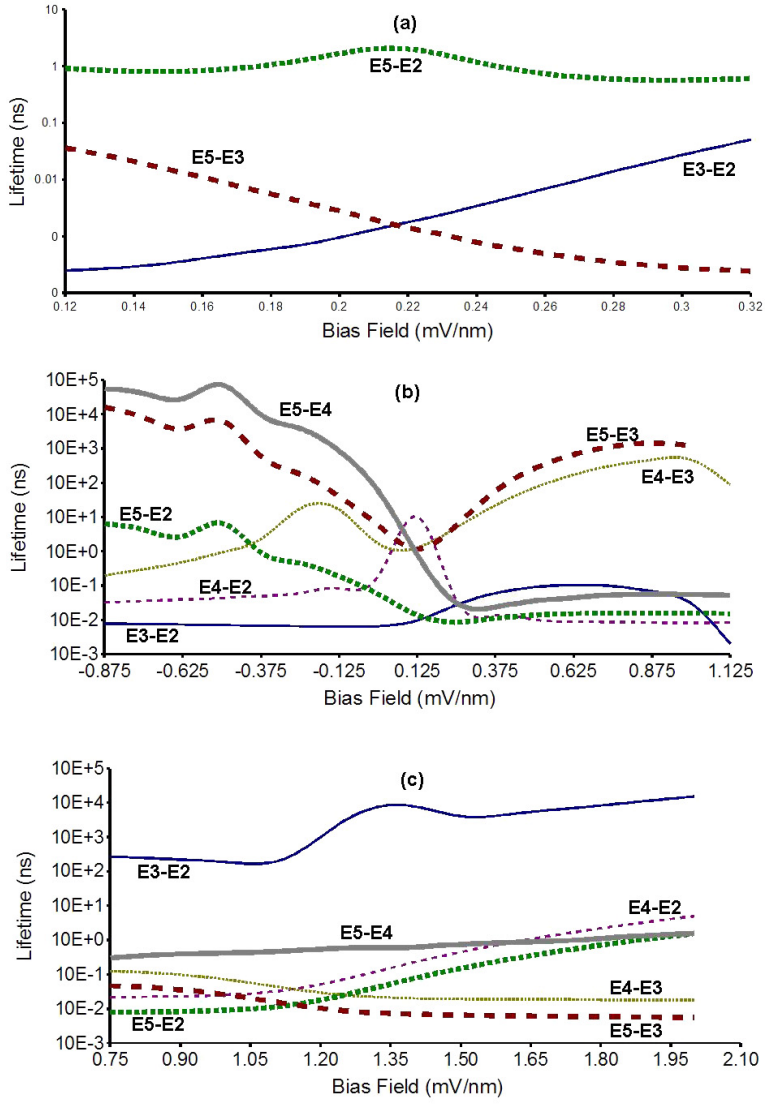

Figure 5. Electron–electron decay times as a function of the bias field for transitions between excited levels: $E2$, $E3$, $E4$ and $E5$ (the transition corresponding to each line is indicated in the plots). (a) Case 1 (spherical double quantum dots), (b) case 2 (laterally coupled double cylindrical quantum dots), and (c) case 3 (vertically coupled double cylindrical quantum dots).

the density matrix, whose evolution is given by the Liouville equation, which in the Lindblad form with the Markovian approximation for the dissipation operator is [48]

$$\mathrm{i}\hbar\frac{\mathrm{d}_{ij}}{\mathrm{d}t} = [H^U(t), \rho(t)]_{ij} - \mathrm{i}\hbar\Gamma_{ij}\rho_{ij}, \tag{8}$$

where ρ_{ij} is the ij density matrix component, H^U_{ij} the matrix element of the Hamiltonian including the exciting electric field, and the constants Γ_{ij} are the relaxation rates calculated in sections 3 and 4.

The pulse we used is a Gaussian one, of the form

$$F(t) = F_0 e^{-(t/\tau)^2} \cos(\omega_0 t), \qquad \tau \leqslant \frac{\hbar}{2\,(E_5 - E_2)}, \qquad \omega_0 = \frac{(E_5 + E_2)}{2\hbar}, \tag{9}$$

where τ has the purpose of making the pulse short enough to interact in the regime of the uncertainty principle, and ω_0 locates it at the central energy between the excited levels to be able of achieving a coherent superposition of those levels. In our calculations we used $\tau = 22$ fs, whose energy uncertainty is enough to cover the excited levels of all the cases.

Solving the equation system (8) after the application of the pulse (9), we calculated the total dipole moment (TDM) between excited states:

$$D_T(t) = \sum_{i,j} d_{ij}\rho_{ji}, \qquad i, j = 2, 3, 4, 5, \tag{10}$$

where d_{ij} are the stationary dipole moments and ρ_{ij} are the coherent superpositions between levels for $i \neq j$, or the populations of levels for $i = j$. Figure 6 shows the TDM calculated for the three studied cases in the HDR using three different amplitudes of pulses.

An oscillating dipole moment means coherent electromagnetic radiation, and figure 6 indicates that for cylindrically shaped dots, especially for those coupled vertically, the observation of such emission is feasible since many cycles are completed before the inhibition by scattering by phonons and conduction electrons [49]. The improvement of the amplitude of the oscillation with the magnitude of the applied field, as would be expected, is also clear.

As we said before, if there were more than one electron confined in the dots, the electron–electron interaction would be expected to be even orders of magnitude larger, which would notably affect the possibility of having this emission according to what happened for the spherical case. So occupation control becomes critical for eventual measurements.

Quantum beat emitters have been studied in three levels, where just one frequency is obtained because only one transition is involved [50–52]. Here, due to the five levels that are considered, up to six different frequencies are possible (three in the spherical case, because two levels remain degenerated), although some of them are quickly inhibited.

6. Conclusions

One-electron dynamics in double spherical and cylindrical quantum dots has been studied in this work. Eigenenergies and envelope functions were found for finite electronic confinement. Relaxation times associated with decoherence processes by electron–phonon and electron–electron calculations were evaluated at room temperature. By tuning with the external bias field we found regions of high electronic delocalization where the relaxation rates are expected to dominate over the pure dephasing rates [53].

Maxima and minima were observed in the decay times of the three systems studied [54], with characteristic lifetimes longer than those in related systems like double quantum wells [55, 56].

Feasible conditions for coherent emission were found in cylindrical dots, particularly when they are vertically coupled (case 3), since this geometry helps the balance between scattering by electron–electron and electron–phonon interactions. The spherical geometry was not found to be suitable to observe coherent emission since the attenuation rate is bigger than the emission frequencies. This is due mainly to the large electron–electron scattering rates associated with this highly symmetric geometry.

The emission frequencies lie in a range from microwaves up to terahertz, which is useful for the spectroscopy of close levels, as has already been applied using magnetic fields in

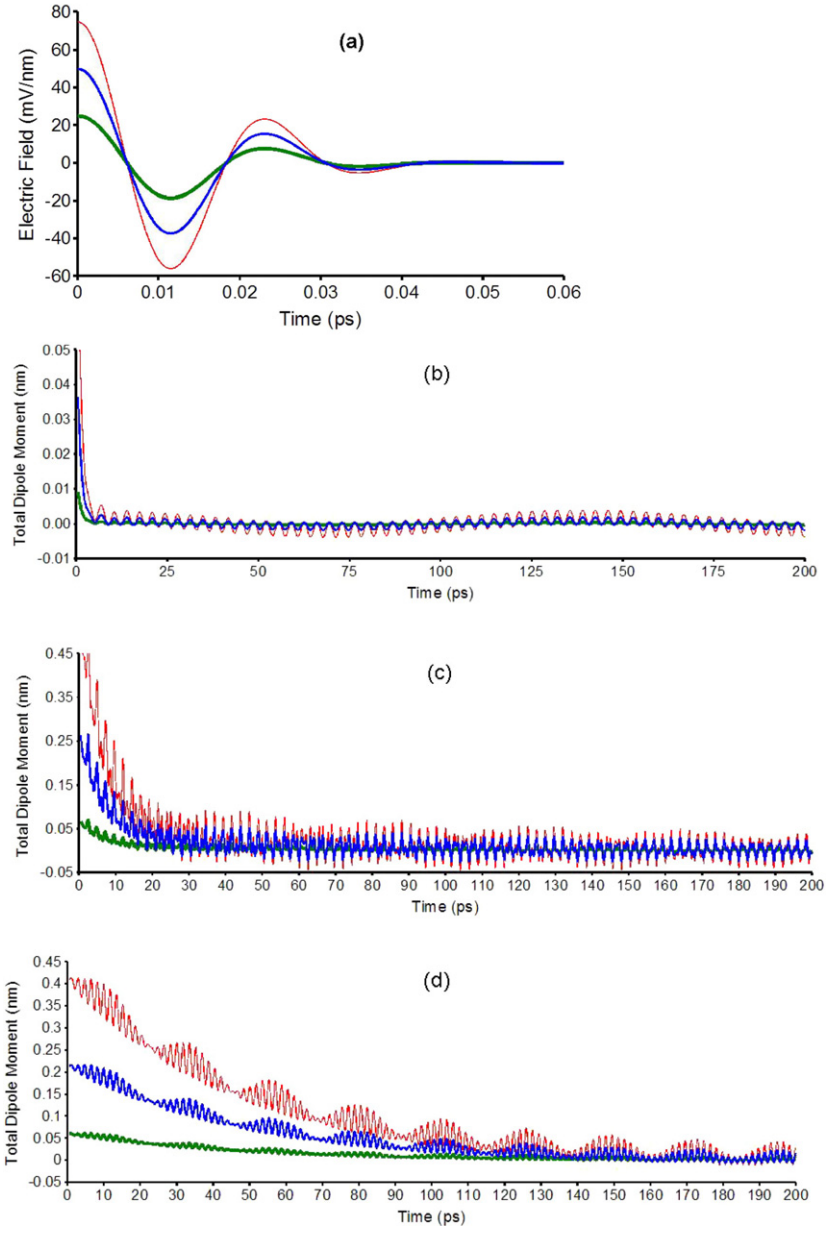

Figure 6. (a) Electric field pulse (red, solid: $F_0 = 75$ mV nm^{-1}; blue, bold: $F_0 = 50$ mV nm^{-1}; green, ultra-bold: $F_0 = 25$ mV nm^{-1}). Total dipole moment at the HDR for (b) double spherical dots ($F = 0.22$ mV nm^{-1}), (c) laterally coupled double cylindrical dots ($F = 0.125$ mV nm^{-1}), and (d) vertically coupled double cylindrical dots ($F = 1.25$ mV nm^{-1}). The colours and line widths for different values of F_0 in (b), (c) and (d) are the same as in (a).

single quantum dots. This kind of coherent emission has been measured in double quantum wells in [57], and now, according to our results, it should be expected in double-quantum-dot systems.

Acknowledgments

We would like to thank the Comite de Investigaciones y Posgrado, y Departamento de Física of Universidad de Los Andes, Colciencias Colombia (Project No: 1204-05-46852), Banco de La Republica Colombia (Project No. 2139), and Wright State University and the Ohio Board of Regents (Research Challenge Grant) for financial support.

References

[1] Nakamura Y, Pashkin Yu A and Tsai J S 1999 *Nature* **398** 786
[2] Mowbray D J and Skolnick S M 2005 *J. Phys. D: Appl. Phys.* **38** 2059
[3] Villas-Boâs J M, Govorov A O and Ulloa S E 2004 *Phys. Rev.* B **69** 125342
[4] Stavrou V N and Hu X 2005 *Phys. Rev.* B **72** 075362
[5] Puska M J, Ogando E and Zabala E 2001 *Phys. Rev.* B **64** 033401
[6] Bertoni A, Rontani M, Goldoni G, Troiani F and Molinari E 2005 *Physica* E **26** 427
[7] Brunner K, Bockelmann U, Abstreiter G, Walther M, Böhm G, Tränkle G and Weimmann G 1992 *Phys. Rev. Lett.* **69** 3216
[8] Li X, Wu Y, Steel D G, Gammon D and Sham L J 2004 *Phys. Rev.* B **70** 195330
[9] Inoshita T and Sakaki H 1997 *Phys. Rev.* B **56** 4355
[10] Borri P, Langbein W, Schneider S and Woggon U 2001 *Phys. Rev. Lett.* **87** 157401
[11] Norris T B, Kim K, Urayama J, Wu Z K, Singh J and Bhattacharya P K 2005 *J. Phys. D: Appl. Phys.* **38** 2077
[12] Nielsen T R, Gartner P and Jahnkel F 2004 *Phys. Rev.* B **69** 235314
[13] Miller B T, Hansen W, Manus S, Luyken R J, Lorke A, Kotthaus J P, Huant S, Madeiros-Ribeiro G and Petroff P M 1997 *Phys. Rev.* B **56** 6764
[14] Ciorga M, Sachrajda A S, Hawrylak P, Gould C, Zawadzki P, Jullian S, Feng Y and Wasilewski Z 2000 *Phys. Rev.* B **61** R16315
[15] Krenner H J, Sabathil M, Clark E C, Kress A, Schuh D, Bichler M, Abstreiter G and Finley J J 2005 *Phys. Rev. Lett.* **94** 057402
[16] Ramirez H Y, Camacho A S and Lew Yan Voon L C 2006 *Braz. J. Phys.* **36** 869
[17] Park G, Shchekin O B, Huffaker D L and Deppe D G 1998 *Appl. Phys. Lett.* **73** 3351
[18] Golovach N, Borhani M and Loss D 2006 *Phys. Rev.* B **74** 165319
[19] Nomoto K, Ugajin R, Susuki T and Hase I 1996 *J. Appl. Phys.* **79** 291
[20] Fedichkin L, Yanchenko M and Valiev K A 2000 *Nanotechnology* **11** 387
[21] Bayer M, Hawrylak P, Hinzer K, Fafard S, Korkusinski M, Wasilewski Z R, Stern O and Forchel A 2001 *Science* **291** 451
[22] Bester G and Zunger A 2005 *Phys. Rev.* B **71** 075325
[23] Bester G and Zunger A 2005 *Phys. Rev.* B **72** 165334
[24] Colombelli R, Ciuti C, Chassagneux Y and Sirtori C 2005 *Semicond. Sci. Technol.* **20** 985
[25] Vardi A, Akopian N, Bahir G, Doyennette L, Tchernycheva M, Nevou L, Julien F H, Guillot F and Monroy E 2006 *Appl. Phys. Lett.* **88** 143101
[26] Koppens F H L, Buizert C, Tielrooij K J, Vink I T, Nowack K C, Meunier T, Kouwenhoven L P and Vandersypen L M K 2006 *Nature* **442** 766
[27] Ramirez H Y, Camacho A S and Lew Yan Voon L C 2006 *Nanotechnology* **17** 1286
[28] Htoon H, Hollingworth J A, Malko A V, Dickerson R and Klimov V I 2003 *Appl. Phys. Lett.* **82** 4776
[29] Hu J, Li L-S, Yang W, Manna L, Wang L-W and Alivisatos A 2001 *Science* **15** 2060
[30] Szafran B, Adamowski J and Stébé B 1998 *J. Phys.: Condens. Matter* **10** 7575
[31] Atoyan M S, Kazaryan E M and Sarkisyan H A 2004 *Physica* E **22** 860
[32] Ioffe Physico Technical Institute New Semiconductor Materials Data Base http://www.ioffe.ru/SVA/NSM/Semicond/index.html
[33] Lew Yan Voon L C and Ram-Mohan L R 1994 *Phys. Rev.* B **50** 14421
[34] Heitz R, Mukhametzhanov I, Stier O, Madhukar A and Bimberg D 1999 *Phys. Rev. Lett.* **83** 4654
[35] Sellami K and Jaziri S 2005 *Superlatt. Microstruct.* **37** 43
[36] Hameau S, Guldner Y, Verzelen O, Ferreira R, Bastard G, Zeman J, Lemaitre A and Gerard J M 1999 *Phys. Rev. Lett.* **83** 4152
[37] Preisler V, Grange Ferreira T R, de Vaulchier L A, Guldner Y, Teran F J, Potemsky M and Lemaitre A 2006 *Phys. Rev.* B **73** 075320

[38] Zibik E A, Wilson L R, Green R P, Bastard G, Ferreira R, Wells J R, Phillips P J, Carder D A, Cockburn J W, Skolnick M S, Steer M J and Hopkinson M 2004 *Phys. Status Solidi* c **1** 2613
[39] Openov L A 2004 *Phys. Rev. Lett.* **93** 158901
[40] Bertoni A, Rontani M, Goldoni G and Molinari E 2005 *Phys. Rev. Lett.* **95** 066806
[41] Bruus H, Flensberg K and Smith H 1993 *Phys. Rev.* B **48** 11144
[42] Sellami K and Jaziri S 2006 *Mater. Sci. Eng.* C **26** 555
[43] Wu Z-J, Zhu K-D, Yuan X-Z, Jiang Y-W and Zheng H 2005 *Phys. Rev.* B **71** 205323
[44] Becker C, Vasanelli E and Sirtori C 2004 *Phys. Rev.* B **69** 115328
[45] Santos D R Jr, Qua F, Alcaldeb A M and Moraisc P C 2005 *Physica* E **26** 331
[46] Nielsen T R 2005 Carrier–carrier and carrier–phonon scattering in self-assembled quantum dots *PhD Dissertation* University of Bremen, Germany p 95, 108
[47] Diniz G S, Qu F, Diniz Neto O O and Alcalde A M 2006 *Braz. J. Phys.* **36** 372
[48] Villas-Boâs J M, Ulloa S E and Govorov A O 2005 *Phys. Rev. Lett.* **94** 057404
[49] Vasko F and Kuznetsov A 1999 *Electronic States and Optical Transitions in Semiconductor Heterostructures* (New York: Springer) pp 268, 282, 285–287
[50] Leo K, Damen T C, Shah J and Köhler K 1990 *Phys. Rev.* B **42** 11359
[51] Vasko F, Hernandez-Cabrera A and Aceituno P 2004 *Semicond. Sci. Technol.* **19** S179
[52] Bohórquez J and Camacho A S 2002 *Braz. J. Phys.* **32** 356
[53] Fedichkin L and Fedorov A 2004 *Phys. Rev.* A **69** 032311
[54] Ramirez H Y, Camacho A S and Lew Yan Voon L C 2007 *Phys. Status Solidi* c **4** 433
[55] Sekine N, Hirakawa K and Arakawa Y 1998 *Japan. J. Appl. Phys.* **37** 1643
[56] Wolter F, Roskos H G, Haring Bolivar P, Bartels G, Kurz H, Köhler K, Grahn H T and Hey R 1997 *Phys. Status Solidi* b **204** 83
[57] Luo Marie S, Cheng Lien Chuang, Planken P C, Brener I and Nuss M C 1993 *Phys. Rev.* B **48** 11043